Chapter 12

Integrated FEA and Raytracing in Instrumentation for Astronomy: Smart Structures Evaluation and Structural Optimization

Marco Riva

Additional information is available at the end of the chapter

http://dx.doi.org/10.5772/47325

1. Introduction

The astronomical instrumentation needs high level of image quality and stability. The quality of images processed by an optical instrument can be referred to the size of the spot and/or the point spread function (p.s.f.), while the stability is related to the displacement of the spot centroid during the observations.

The opto-mechanical elements are designed and manufactured in order to have enough stiffness to minimize shape deformations and flexures due to thermo-gravitational loads. Old traditional design philosophy answered to the problem with high thicknesses and related high masses. Heavier glasses means heavier supports and high gravitational dependent misalignment. The technological research is nowadys devoted to the light weighing of opto-mechanical systems either keeping enough stiffness, or actively correcting optical surfaces and/or positions. Complementary to the technological research, the development of powerful numerical tools added to an huge enlargement of CPU computing capacity have been offered a significant improvement into the engineering design enhancing the complexity and efficiency of the design phase.

Optical lens design refers to the calculation of lens construction parameters (variables) that will meet a set of performance requirements and constraints, including cost and schedule limitations. Construction parameters include surface profile types (spherical, aspheric, holographic, diffractive, etc.), and the parameters for each surface type such as radius of curvature, distance to the next surface, glass type and optionally tilt and decenter. The optical design exploits numerical raytracing techniques to maximize the design efficiency. Ray tracing is a method for calculating the path of waves or particles through a system with regions of varying propagation velocity, absorption characteristics, and reflecting surfaces. Under these circumstances, wavefronts may bend, change direction, or reflect off surfaces, complicating analysis. Ray tracing solves the problem by repeatedly advancing idealized narrow beams called rays through the medium by discrete amounts. Simple problems can be analyzed by

propagating a few rays using simple mathematics. More detailed analyses can be performed by using a computer to propagate many rays.

On the other hand, structural design is nowadays mainly based onto The finite element method (FEM). It is a numerical technique for finding approximate solutions of partial differential equations (PDE) as well as of integral equations. The solution approach is based either on eliminating the differential equation completely (steady state problems), or rendering the PDE into an approximating system of ordinary differential equations, which are then numerically integrated using standard techniques such as Euler's method, Runge-Kutta, etc.

The optimization procedure refers to choosing the best element from some set of available alternatives. In the simplest case, this means solving problems in which one seeks to minimize or maximize a real function by systematically choosing the values of real or integer variables from within an allowed set. This formulation, using a scalar, real-valued objective function, is probably the simplest example; the generalization of optimization theory and techniques to other formulations comprises a large area of applied mathematics. More generally, it means finding "best available" values of some objective function given a defined domain, including a variety of different types of objective functions and different types of domains.

In this chapter we present a possible simplified application of the optimization theory to opto-mechanical design that has been integrated into a multipurpose combined opto-mechanical numerical design process. In particular we will show a single variable optimization routine oriented to minimize mass while keeping the optical displacement below a certain value [12]. In addition considering the general purpose of this book will be briefly shown the modeling techniques used in some application to simulate the performances of functional materials like SHape Memory Alloys and Piezoelectrics. This techniques has been implemented in the optimization algorithm to maximize the efficiency of this devices in the actuation of active Mirrors based onto composite materials.

2. Framework

The integrated design procedure proposed exploits the huge power of numerical computation for the design of instrumentations for astronomy. The framework can be ideally seen as "server to client" communication, where a managing server code feeds input data to computing clients and extracts the desired results. The adopted software are:

- Matlab® is the server software: it adapts the inputs for the client codes and evaluates their outputs.
- MSC-Nastran® is the FEA client code: it receives from the server code proper models and computes mechanical results (thermo-gravitational displacements, eigen-frequencies, ...)
- ABAQUS® is a FEA client code used alternatively to MSC-Nastran® in case of user defined contitutive laws.
- Zemax® is the Raytracing client code: it receives the optical perturbations properly adapted and evaluates the optical performance of the system (image quality, image stability, ...).

The procedure obtains image quality and motion of an opto-mechanical system under thermal and/or gravitational loads. A simplified mesh (1d or 2d elements) of a possible

opto-mechanical configuration is prepared starting from the optical design. Then Matlab® implement physical properties into the input file and feeds the MSC-Nastran® solver. The displacements are extrapolated and reorganized in order to be compliant with the Zemax® reference systems. Matlab® runs the Zemax® solver and extract the desired data (Spot radius, EE80, p.s.f., ...). In this way a first order estimation of the Instruments mechanical stability is obtained and can be easily implemented an optimization process based onto the smart modification of the physical and mechanical properties depending onto the Zemax® results.

Easy modifications can be introduced to improve the accuracy of the algorithm's results. A "`qr`" based Zernike fitting function has been implemented in order to allow the modeling of optical surface deformations introducing surface errors into the Zemax optical layout. This configuration can be used both for overall system analysis and for detailed object analysis like active optical element performances evaluation[11, 13].

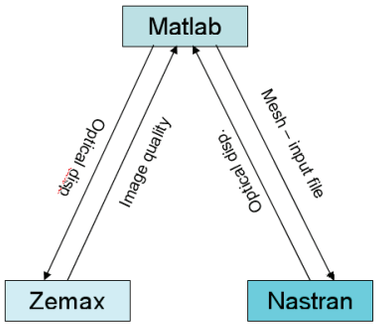

Figure 1. Numerical Framework

2.1. FEA

2.1.1. Mesh generator

The opto-mechanical Finite Element modeling starts from the optical model. Masses, Center of Gravity and Optical Centers of each element are extracted from the optical file. A simplified Matlab® discretization function can be used when the instrument is very simple (i.e. two or three elements); in case of complex geometries the preliminary mesh can be prepared through dedicated software (Femap® , Hypermesh® , ...); this raw discretization usually models a bench or a box that profiles the optical systems through 2D elements. Due to the high interaction level required we decide to omit the automation of the whole bench meshing.

The opto-mechanical elements are then modeled through semi-rgid elements and concentrated masses. The weight of opto-mechanical subsystem is simplified considering double the optical element mass to include the contribution of mechanical mountings. The semi-rigid element (80%) is used instead of the rigid one in order to simulate the finite stiffness of the mountings; the master node is the optical vertex and the slave are the system's CoG and the connection points. Depending onto the geometry and the interface of the instruments, sometimes it is necessary to introduce some reinforcement beams or support trusses that can be easily modeled through 1d beam elements. In some cases, in particular with large optics or

active optical systems, it is important to model the whole optical surface through 2D elements connected to the main bench via 1D beams.

Matlab® can read the model mesh and writes the input file for the Finite Element processor modifing both the geometry and the properties (thickness of 2D and section of 1D elements) if needed. This feature is the crucial point that helps the designer to optimize the performances of the system.

Different codes can be used for different application. The interaction with ABAQUS[1] is necessary for smart structures applications thanks to the higher performances of the code in presence of user defined constitutive laws. The routines interacts with NASTRAN[6] for opto-mechanical performances prediction and optimization.

2.1.2. Fast extrapolation algorithm

To evaluate the whole performances of an instrument is necessary to verify the performances within all the loading conditions. In particular it should be possible to find situations where the errors tends to auto-compensate or, on the other hand, are magnified by the interaction with other perturbations.

Here is presented a simple extraction algorithm that can be used to reduce the number of FEA analysis required. The basic idea is to perform less analyses as possible and extracts all the displacement fields in an analytical way. Doing this, one can also predict the displacements in every condition of the gravitational load with or without the thermal expansion.

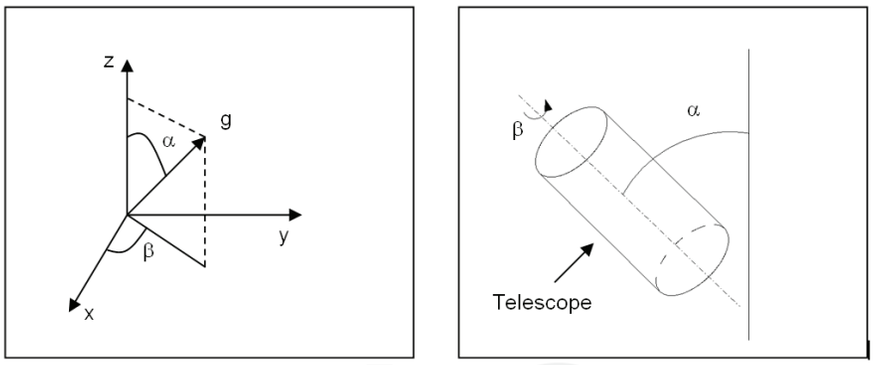

Figure 2. Reference systems

If the g vector rotates in the whole 3D space the analytical definition of the displacements is more complex. First of all it is necessary to define how decompose the $g$vector in the three directions x, y and z. We have decided to use that shown in Figure 2. In this way we can simulate the real rotations of the telescope, the α angle is the declination and β angle represents the rotation of the telescope around the optical axis. Doing this, the components of the g-vector are:

$$\begin{cases} g_x = & g \cdot sin(\alpha) \cdot cos(\beta) \\ g_y = & g \cdot sin(\alpha) \cdot sin(\beta) \\ g_z = & g \cdot cos(\alpha) \end{cases} \tag{1}$$

The equation that ties force and displacements can be written as:

$$D = K^{-1} \cdot F \tag{2}$$

Where D is the displacements vector, K the stiffness matrix, and F is the loads vector. If we combine Equations 1 ans 2, through some algebraical operations, we obtain the general form:

$$D = A_1 \cdot sin(\alpha) \cdot sin(\beta + \phi) + A_2 \cdot cos(\alpha) \tag{3}$$

Where A_1 is the vector of the maximum amplitudes of the displacements when the g vector is in the xy plane, A_2 is the vector of the maximum amplitudes of the displacements when the g vector is orthogonal at the xy plane, α and β are the angles of equation 1 and ϕ is a phase vector of the sinusoids. In order to have the whole displacement we need three known points to determinate the three unknown variables: the amplitudes and the phase.

Equation 2 can be further detailed introducing the thermal loads simply by adding the $C \cdot T$ term, where C C is a vector constant which ties the temperature T at the displacement D. If we consider T_d as the the vector of the displacements due to the thermal loads, Equation 3 becomes:

$$D = A_1 \cdot sin(\alpha) \cdot sin(\beta + \phi) + A_2 \cdot cos(\alpha) + T_d \tag{4}$$

Now with only four known points (for four unknown variables: the two amplitudes, the phase and the thermal displacement) we can have the overall displacements and the possibility to decompose the thermal contribution.

In addition we should note that Equation 4 can be simplified if the known points are wisely taken. In fact if the sampling loading condition are:

1. $\alpha = 90$, $\beta = 0$, $\delta T = 0$: gravity vector along X axis, no thermal load.
2. $\alpha = 90$, $\beta = 90$, $\delta T = 0$: gravity vector along Y axis, no thermal load.
3. $\alpha = 0$, $\beta = 0$, $\delta T = 0$: gravity vector along Z axis, no thermal load.
4. $g = 0$, $\delta T \neq 0$: only thermal load.

The algebraic simplification of Equations 1 and 2

$$D = X \cdot sin(\alpha) \cdot cos(\beta) + X \cdot sin(\alpha) \cdot sin(\beta) + Z \cdot cos(\alpha) + T_d \tag{5}$$

2.1.3. Zernike fitting

The surface Deformations are processed through a Zernike Fitting algorithm. In precision optical manufacturing, Zernike polynomials are used to characterize higher-order errors observed in interferometric analysis, in order to achieve desired system performance. They are commonly used in active and adaptive optics where they can be used to describe wavefront aberrations.

The most general way to express the Zernike polynomials is in the form:

$$R_n^m(\rho)e^{im\theta} = \begin{cases} R_n^m(\rho)cosm\theta \\ R_n^m(\rho)sinm\theta \end{cases} \tag{6}$$

Where the n index defines the order of the radial power so an n value of 5 would indicate all polynomials whose maximum radial power is ρ^5. Only certain values for m are allowed once n is chosen; $n + m$ must be even, and $0 \leq m \leq n$. The surface error is defined as[2]:

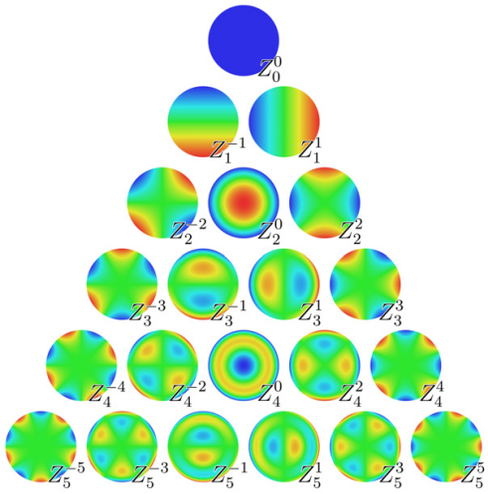

Figure 3. Zernike polynomial basis

$$E = \Sigma(\delta_i - D_i)^2 \tag{7}$$

where i is the node number, δ_i is FE displacement of i_{th} node, D_i is the polynomial displacement of the i_{th} node. The series of D can be symbolically written as $D_i = \Sigma c_j f_{ij}$ where c_j are the coefficients of the polynomial. The best fit coefficients can be found minimizing the error E respect to c_j:

$$\frac{dE}{dc_j} = 2\Sigma(\delta_i - \Sigma c_j f_{ij}) f_{ij} = 0 \tag{8}$$

This system is then solved finding the best fitting coefficients through an orthogonal-triangular decomposition (Matlab® *qr* function). The first 28 coefficients of the Zernike Polynomial have been taken into account in this application.

2.2. Raytracing

2.2.1. Zemax® and Matlab® data exchange

The raytrancing software Zemax® is used to evaluate the optical performances. Zemax® has a very powerful feature which allows another software to establish a communication link to extract lens data. The idea is based onto a program that use Zemax® like a remote application to trace rays through the lenses, and then extracts the data to be sent to other programs for further analysis or computation[17].

The communication between the application and Zemax® is accomplished using Dynamic Data Exchange (DDE). DDE is a protocol defined within the Windows operating system for sharing data between programs. Two programs can establish a DDE link, with one program acting as the "server" and the other the "client". The client generally requests specific data from the server, and the server sends the data back to the client.

Two main function must be used when exchanging data with Zemax that are the link opening and closing. To establish a DDE link with Zemax® , the client program must broadcast a message to all top level windows that includes a reference to the application name, and the topic name. The topic name indicates to Zemax® what data is being requested.

Zemax® supports a number of capabilities under DDE. Each function/item is given a name, that is passed to the Zemax® server using the proper request protocol. Zemax® responds to each item request with requested data. Most of them are passed from Zemax® back to the application (Matlab®) in a string that must be properly managed.

2.2.2. Zemax® computations

In the case of thermal and gravitational performances evaluation, it is necessary an adaptation of the optical model. Coordinate Breaks (CB) are introduced before and after each Optical element paying attention to the transformation sequence. This is crucial to realize a feature that allow the introduction of local optical displacements without modifying the remaining optical layout. Matlab® extracts optical displacements from Nastran (global coordinate system), optical coordinate systems from Zemax® and applies the proper transformation matrices to obtain optical displacements in Zemax® local reference systems. In case of surface deformations, the surfaces of Zemax® file are modified from "Standard" to "Zernike Fringe Sag" in order to allow Matlab® to updates the extra data tables with the Zernike coefficients obtained from the fitting algorithm.

After the uploading of mechanical data into the optical file, Zemax® evaluate spot and p.s.f. information through its raytracing engine. If necessary Matlab® request a focusing optimization after having stored the focal plane distance to evaluate the relative focal variation. Finally Matlab® extract from Zemax Spot dimensions (Max and R.M.S. radius) and centroid displacement, eventually of multiple fields.

The results defines respectively the image quality and stability of the overall optical layout and, if necessary can be passed to an optimization algorithm that manage the mechanical properties of the system.

2.3. Optimization

Whereas optimization methods are nearly as old as calculus, numerical optimization reached prominence in the digital age. Its systematic application to structural design dates to its advocacy by Schmit in 1960. The success of structural optimization in the 1970s motivated the emergence of multidisciplinary design optimization (MDO) in the 1980s. Here will be presented a simplified single variable optimization approach that has been used as starting point[14].

2.3.1. Problem statement

The general optimization problem (for example minimization) wants to minimize the objective function:

$$F(X) \tag{9}$$

subjected to inequality constraints:

$$p_j(X) \leq 0 \quad j = 1 : m \tag{10}$$

and equality constraints:

$$h_k(X) \leq 0 \quad k = 1 : l \tag{11}$$

and side constraints (if applicable):

$$X_i^l \leq X_i \leq X_i^u \quad i = 1 : n \tag{12}$$

where vector X is the n dimension design variable vector.

In opto-mechanical variable design X may consists into the instrument properties (shell thickness, beam diameter, ...) while $F(X)$ is the overall instrument Mass function dependent to design variables. The inequality constraint $p(X) \leq 0$ is the optical displacement that must be kept within certain specifications.

2.3.2. Iterative procedure

The optimization algorithm requires an initial set of variables X_0. In the opto-mechanical optimization we consider as staring point the preliminary mesh defined by the user based onto its own experience. The whole integrated analysis is carried out as shown in this chapter extracting from MSC-Nastran® the overall system mass and from Zemax® the first optical displacement set. A small perturbation is applied onto the design variable ($X_1 = X_0 + \delta X$) and the procedure evaluates a second set of Mass and optical displacements. After the initialization the gradient of Mass and Optical displacement functions are evaluate respect to the design variable and the automatic procedure is started.

The optimization routine is launched:

1. Evaluate Mass function gradient as $\nabla M(X_{i-1}) = (M(X_{i-1}) - M(X_{i-2}))/(X_{i-1} - X_{i-2})$;
2. Update the design variable: $X_i = X_{i-1} - g_M \nabla M(X_{i-1})$ where g_M is a gain factor properly set in order to manage iteration number;
3. Evaluate Mass and optical displacement with new variables and update step counter;
4. Is optical displacement below specification? Yes: go to point 5; No: go to point 6
5. Is $M(X_i) - M(X_{i-1}) \leq Toll$ (where $Toll$ is a reference value) i.e. the minimization converging? Yes: optimization ended; No: go to point 1
6. Evaluate Displacement function gradient as $\nabla D(X_{i-1}) = (D(X_{i-1}) - D(X_{i-2}))/(X_{i-1} - X_{i-2})$;
7. Update the design variable: $X_i = X_{i-1} - g_D \nabla D(X_{i-1})$ where g_D is a gain factor properly set in order to manage iteration and go to point 3

3. Modeling techniques

In the attitude of this book, following will be presented the modeling technique developed for the build up of the Finite Element Models of the Smart Structures. In particular the techniques adopted for the modeling of PiezoComposites and Shape Memory Alloy will be briefly introduced. It will not be described here the phsyical behaviour of the materials, detialed description of the full work and approach can be found in [11] and in [13].

3.1. Shape memory alloy Finite Element modeling: the Turner micro-mechanical approach

To perform Finite Element analysis regarding SMA is necessary to define the proper constitutive law that describe the material behavior. In this paper will be presented the FE implementation of three different constitutive law. A further detailed description of the laws and their application can be found in the references [7].

In physics, a constitutive equation is a relation between two physical quantities (often described by tensors) that is specific to a material or substance, and approximates the response of that material to external forces. It is combined with other equations governing physical laws to solve physical problems, like the flow of a fluid in a pipe, or the response of a crystal to an electric field.

During the last ten years researchers have been developed several constitutive laws that can be classified considering the different approaches used in their formulation such as: micro-mechanical or macro-mechanical and phenomenological or thermodynamic.

The micro-mechanical formulation essentially takes into account the properties of single crystals of the material averaging their behavior over a Representative Volume Element (EVE). Micro-mechanical models have been developed using a thermodynamic approach and evaluating the energy involved during a phase transformation. These models also use homogenization techniques to derive the overall behavior of the SMA.

The real benefit of this class of model lies in their ability to predict the real response of the material starting from the lattice parameters for crystalline and crystal and grain level data derived from martensitic transformation. Nevertheless these models are very complex and require a large number of computational operations.

The Turner model has been successfully implemented into the commercial code ABAQUS® [10]. This model defines temperature dependent Young modulus and Thermal expansion coefficient. Exploiting some peculiar properties of the software it is possible to define a look up table mapping the variation of material characteristics. As obtained from the calibration of the model (Figures 4 and 5), it has been used the definition of Young modulus and Thermal Expansion coefficient as a function of temperature.

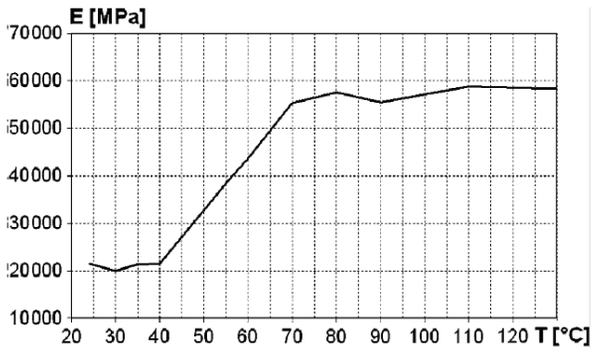

Figure 4. SMA $E(T)$

Different verification models were performed to select the type of the elements [10]. The comparison underlines how a shell model is precise enough with a high gain in terms of CPU time. Due to this consideration, the final comparison was conducted on a shell-based model

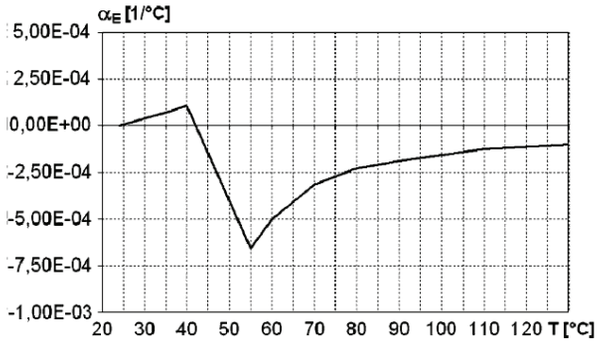

Figure 5. SMA $\alpha(T)$

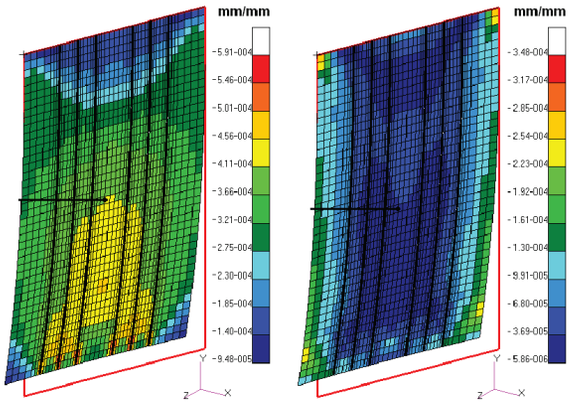

Figure 6. Turner Finite Element model

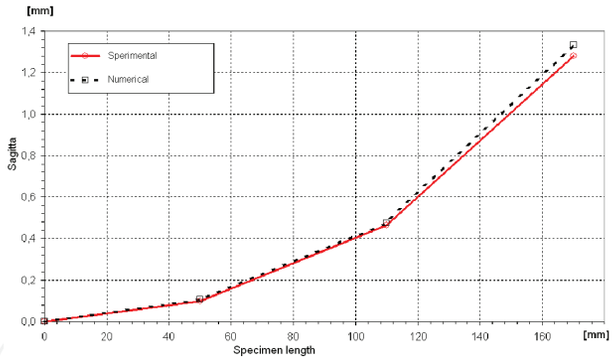

Figure 7. Displacement Turner correlation results

with composite laminate properties. The NiTiNOL actuators were modeled thickening the mesh and considering the material as a "ply" of the lamination sequence. The thermoelastic model receives as input the thermal load on the wires and derives the temperature behavior of all the nodes (Figure 6).

A carbon fiber-reinforced panel with six embedded NiTiNOL wires was modeled and analyzed using the ABAQUS commercial code. The actual panel was manufactured with 12 plies $[90/(0)_2/90/+45/-45]_s$ and its overall dimensions were: 30 x 170 x 1.2 mm. The actuators chosen were OWSME wires ($\phi = 0.38mm$) trained using standard heat treatments. They were embedded between the 2^{nd} and the and 3^{rd} plies with a 4% imposed strain. The manufacturing technolgoy is reported in [3, 10]. The panel was constrained on one side

and activated via Joule effect. The numerical/experimental comparison shows that, after a short transition, the predicted displacement matches (max. error 20 μm) the experimental one (Figure 7).

3.2. Piezoelectric numerical modeling:"Structural-scale" modeling technique for MFC

Following will be presented the numerical technique adopted to model The Macro Fiber Composites (MFC) that have been developed by NASA Langley Research Center (LARC) in 2000 [16]. The components of the MFC are illustrated in Figure 9. The core is made by aligned piezoceramic fiber included in epoxy resin and joined between two groups of interdigited electrodes (IDE) supported by a Kapton film. The MFC have an overall thickness of $0.3mm$ and the dimensions of the region in which are placed PZT fibers called the active area, can vary from an area of $28 \times 14mm^2$ to $85 \times 28mm^2$. The spacing of IDE is $0.5mm$, while the fibers have a width of $350\mu m$ and a volume fraction above 85%.

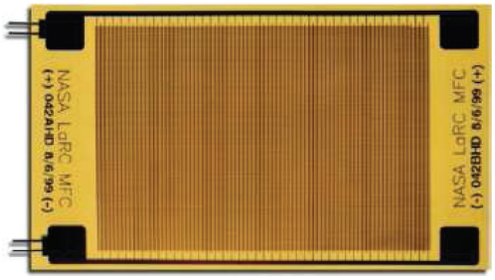

Figure 8. MFC actuator

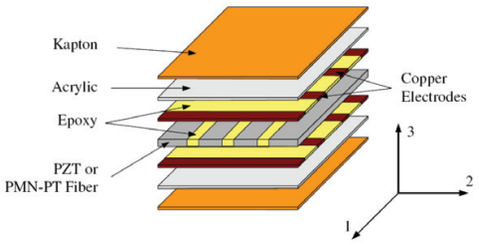

Figure 9. MFC layers

The set up of numerical procedure for the performance prediction as the selection of the best technology to couple the structure to the actuators are fundamental to design efficient smart structures. The numerical approach for the design of piezo based smart structures is dealt in this section . The design of smart structure is mainly oriented to the study of authority and then to the stress analysis. With the intent of reducing the design time, a technique able to predict the overall performances of the structure through "light-weight" numerical models was developed.

The overall smart structure can be conceptually divided into two sub-system: the structure itself consisting into the composite panel and the MFC actuators. The proposed technique is developed under the ABAQUS® commercial code [4] environment[1] and neglect the detailed analysis of stress state adopting essentially two type of elements: `S4R` four-node shell elements for the host material and `C3D20RE` twenty-node quadratic bricks (reduced

[1] And can be obviously ported to other Finite Element Codes

integration[2]) for the actuator. The two subsystems are modeled as separated mesh connected together through the `*TIE` algorithm which introduce a link between the nodes of the two different surfaces evaluating the distances between the two faces and obtaining an adhesion factor to be applied at each node (Figure 10).

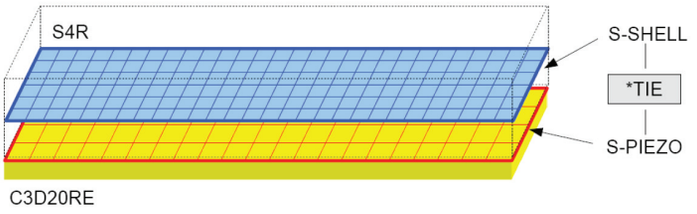

Figure 10. Sketch of the proposed structural scale technique.

Figure 11. Layout for the structural scale validation.

A simple laminate (Figure 11) $200 \times 40mm$ made by three layers, with the piezo in the middle, has been considered to validate the proposed technique. A d.d.p. of $100V$ between the electrodes has been simulated and the transversal motion of the tip has been evaluated through the Classic Lamination Theory (CLT) [4]. Since the laminate is formed by three plates the `TIE` algorithm is used twice. Due to the fact that Piezo element are quadratic, while shell ones are linear different mesh densities must be adopted as shown in Figure 12

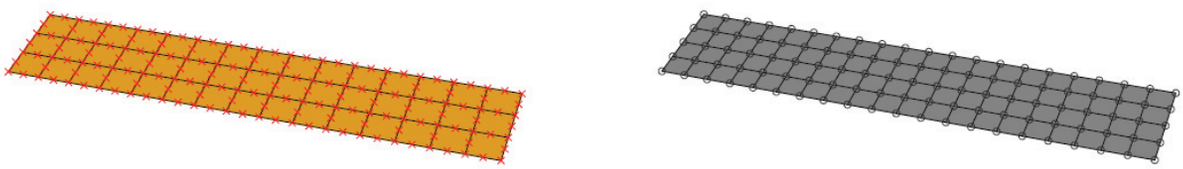

(a) Master (b) Slave

Figure 12. Different mesh densities

It is important to pay attention to the constraint conditions, because those nodes are also influenced by the `TIE` algorithm which connect elements with six degrees of freedom (d.o.f.) per nodes to other with three d.o.f. per nodes. If compared with the CLT, the results coming from those analyses, strongly encourages the use of these techniques in fact the tip deflection error obtained is less then $1e-3\%$.

The proposed technique can be also adopted for the modeling of smart structures with MFC actuators. For an overall performance evaluation is not necessary to model the whole

[2] the reduced integration is necessary to reduce the so called shear-locking numerical induced effect

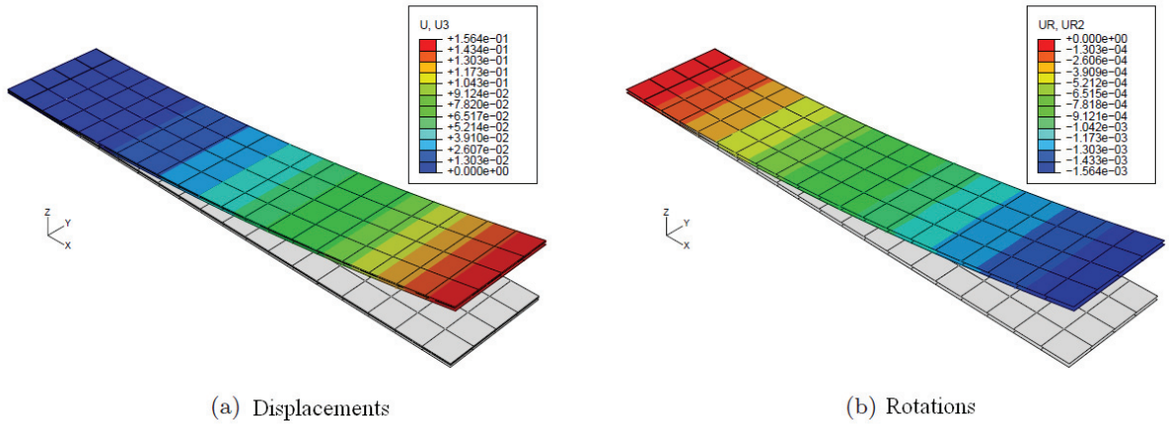

(a) Displacements (b) Rotations

Figure 13. Finite Element results of the test specimen

detailed MFC as a sequence of different layers and subcomponents. A previous comparison [4] between detailed models[3] confirm in fact, that the displacements resulting from the light-weighted technique are exceptionally close to the detailed ones.

The MFC have then been modeled through an homogeneous equivalent piezoelectric plates MFC_{EQ} with the same effective coefficients derived from the data-sheets. The dimensions that have been taken into account are the ones of the active area, while the electrodes have been modeled as a voltage equivalent activation[4].

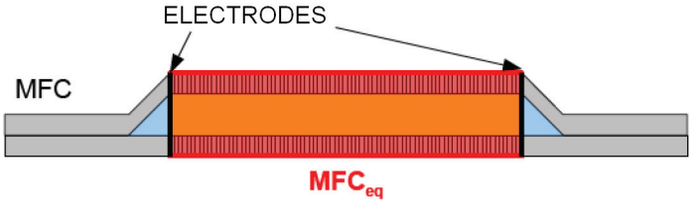

Figure 14. MFC_{EQ} into its MFC counterpart

The MFC_{EQ} has been then used for the modeling of simple smart panels with bonded or embedded actuators. The simply bonding of the piezo device onto a panel is simulated through the `TIE` algorithm and have been compared with the detailed one obtaining limited errors ($1e-2\%$).

4. Applications

4.1. Shape memory actuated deformable mirrors

This procedure has been used to evaluate optical performances deformable mirrors[7–9] based onto new technologies known as smart structures. Carbon fiber reinforced Mirrors actuated by Shape Memory Alloy wires have been modeled to verify their optical capabilities. Image

[3] The whole substructure was modeled in detail with $0.2mm$ mesh pitch
[4] the electric field between two digit times the number of digit gives the overall electric field and tension.

quality during refocusing oriented activation has been evaluated. Several runs of this code has been performed, varying the number/position of actuators and the structure lamination sequence in order to have the evaluation of the influence of each ingredient onto the efficiency of the overall system. In this particular application the routine interact with ABAQUS® that is a finite element solver more reliable with user defined Constitutive laws. The aim of the analysis was the evaluation of the authority of the actuators into the variation of the curvature radius of the shell keeping the image quality within acceptable limits.

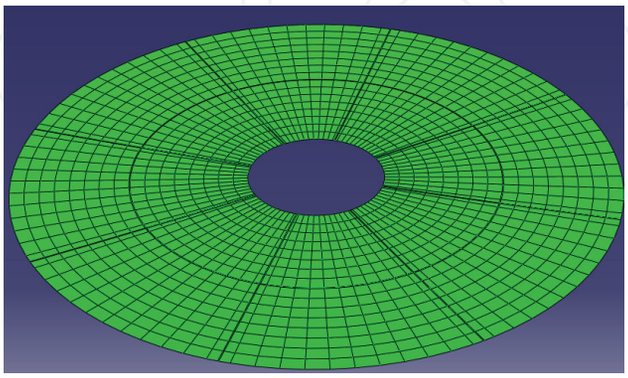

Figure 15. Undeformed SMA actuated Deformable mirror

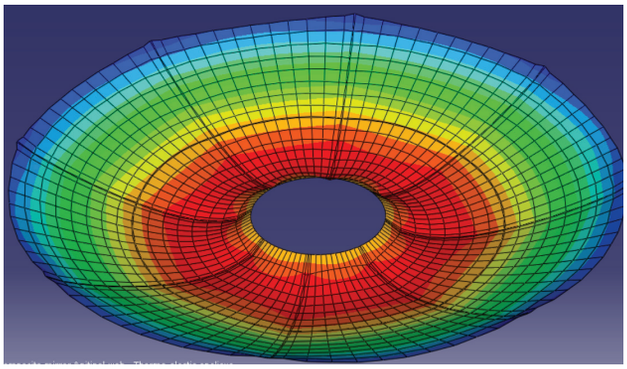

Figure 16. Deformed SMA actuated Deformable mirror

In Figure 17 is shown the overall activation sequence: the first part of the process is dominated by a contraction of the deformable mirror due to the mismatching of the CTE of NiTiNOL respect to CFRP; when the temperature raise up to the A_S the phase transition starts and the actuators imposes the recovery strain deploying the deformable mirror. The image quality has been evaluated both in terms of focusing spot (Figures 19 and 21) and p.s.f. (Figures 18 and 20)

Several analyses have been performed to evaluare the focusing capabilities respect to the number of actuators and the stiffness of the substrate (i.e. number of composite plies). For the detail and the results of this analyses that are not purpose of this chapter we refer to [8]. As an example here we show how the actuators density modify the efficiency of the smart SMA actuated structure. Thus why thw he comparison between two different configurations that offer similar variations of focal positions is shown. In Figure 22 is displayed the overall focusing variation comparing a 48 plies substrate with 14 actuators (blue) and a 36 plies with 8 actuators (green). This behavior has been crosschecked with the RMS and max spot size variation (respectively Figures 23 and 24).

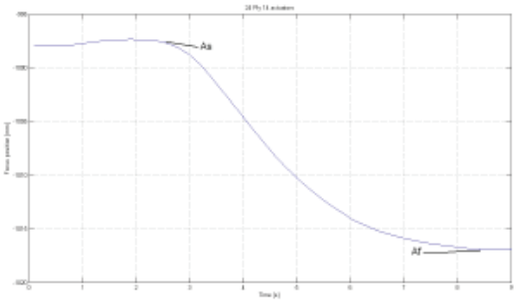

Figure 17. Example of variation of focus position during the activation of a SMA deformable mirror.

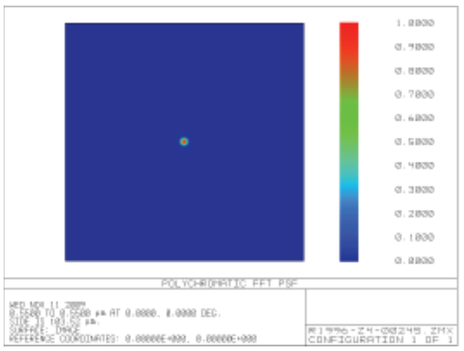

Figure 18. Starting p.s.f.

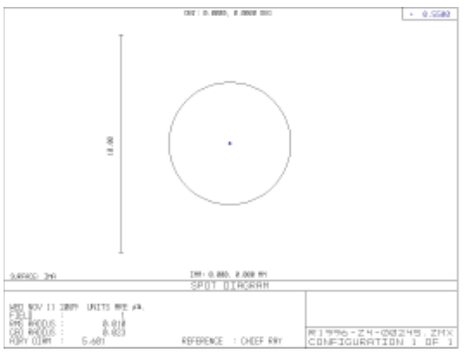

Figure 19. Starting focused spot

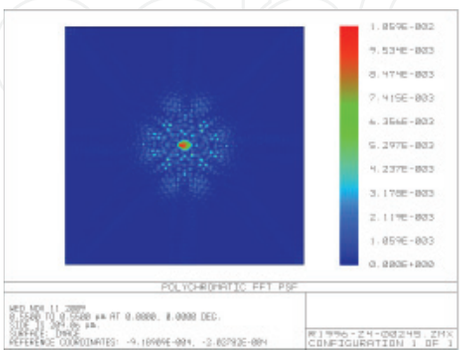

Figure 20. Example of Deformed p.s.f.

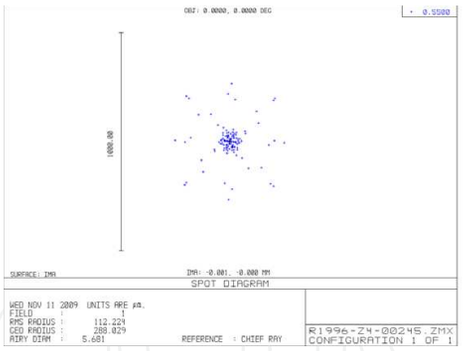

Figure 21. Example Deformed focused spot

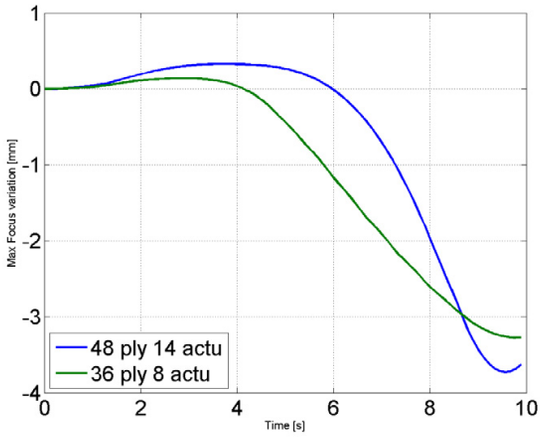

Figure 22. Focal position variation with similar focusing range

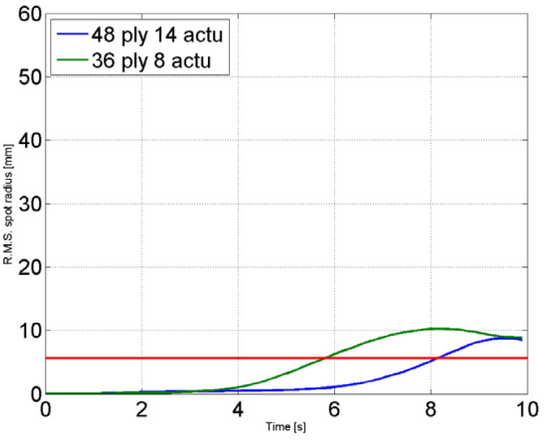

Figure 23. RMS spot radius with similar focusing range

4.2. MFC actuated deformable mirrors

The same approach (paragraph 4.1) has been used to evaluate Carbon fiber reinforced Mirrors actuated by Piezoelectric MFC actuators.

Analyses have been conducted based on the correlation data obtained by the validation of simplified modeling technique presented in Paragraph 3.2. In particular the surface quality

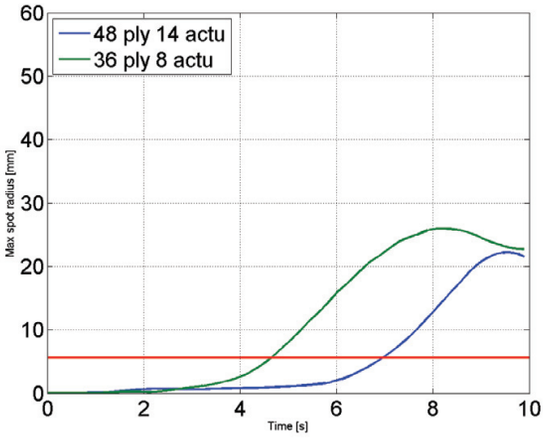

Figure 24. MAx spot radius with similar focusing range

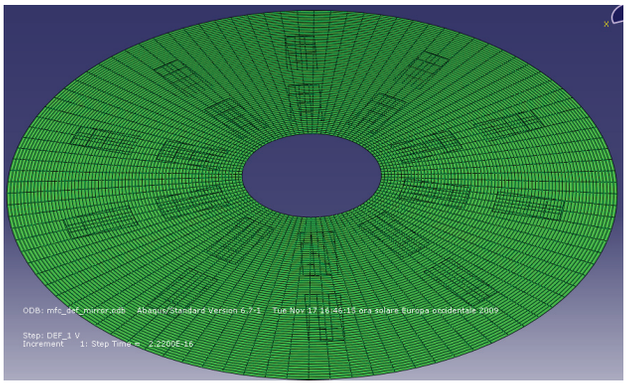

Figure 25. Undeformed Piezo actuated Deformable mirror

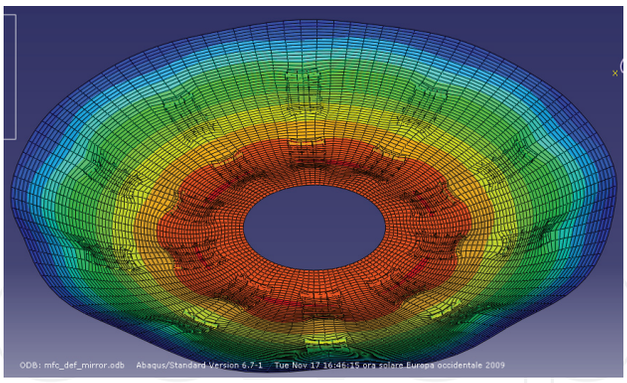

Figure 26. Deformed Piezo actuated Deformable mirror

and the curvature radius variation have been verified as functions of the number of actuators, the different configurations and the lamination sequence.

It has been considered the smallest type of actuator even if the analysis framework set up allow the implementation of several type and dimension of them, simply due to the fact that they were already available in the laboratory,

Considering this class of actuators the performances are not satisfactory when the MFC are placed onto a single concentric ring. In Figures 27, 28 and 29 the results obtained with a population of 15 actuators evaluated as a technological limit are plotted; the radial

coordinates have been parametrically obtained searching for the best performances that have been obtained placing the actuators at 0.53% of the mirror radius. With this layout the spot size goes out of boundary limit with low radius variations ($0.37mm$) while the max spot radius is always unacceptable.

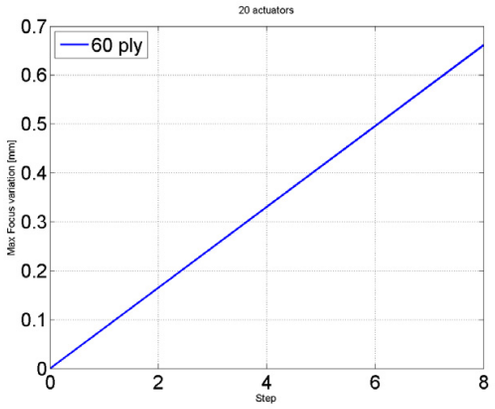

Figure 27. Focal position variation with 10 actuators along one ring (60 plies)

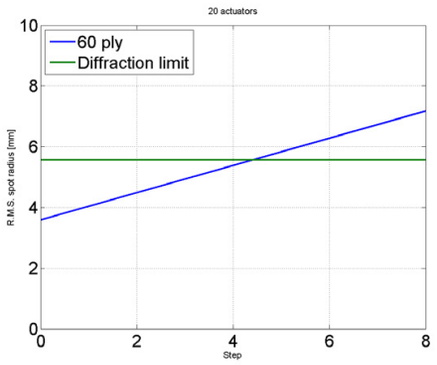

Figure 28. RMS spot radius with 10 actuators along one ring (60 plies)

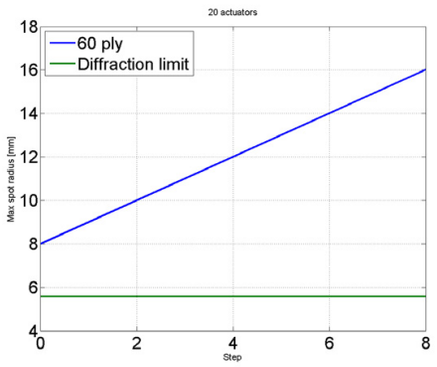

Figure 29. Max spot radius with 10 actuators along one ring (60 plies)

The performance of the piezo actuated smart deformable mirror are more interesting if we consider two ring of actuators, with the same angular coordinates (Figure 25). In Figure 26 is shown the contour of deformation. The results obtained comparing configurations with respectively 8 and 10 batteries of actuators (Figures 30, 31 and 32) shows the more interesting performances, both in terms of higher radius variation and in terms of better image quality

processed, with the higher number of actuator that are then limited only by technological aspects, mainly related to the crowding of the surface.

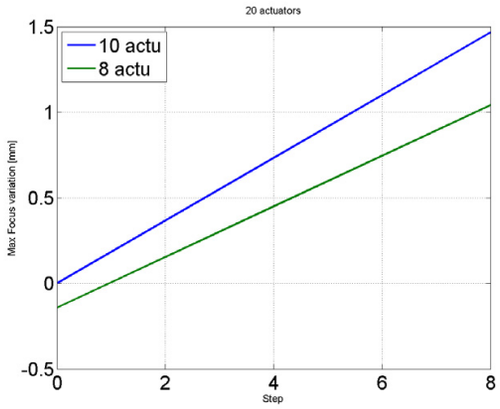

Figure 30. Focal position variation with 10 and 8 actuators per ring (two ring 60 plies)

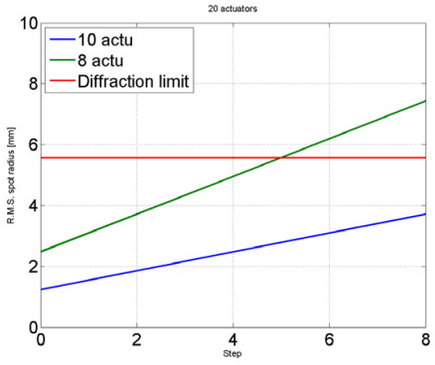

Figure 31. RMS spot radius with 10 and 8 actuators per ring (two ring 60 plies)

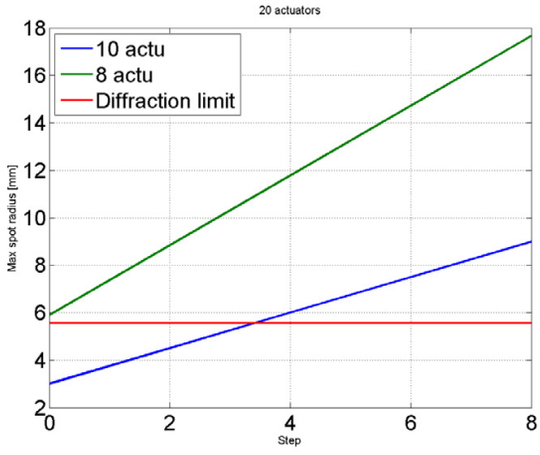

Figure 32. Max spot radius with 10 and 8 actuators per ring (two ring 60 plies

Also in this case have been performed analyses to evaluare the focusing capabilities respect to the number of actuators and the stiffness of the substrate. For the detail and the results of this analyses that are not purpose of this chapter we refer to [8].

4.3. Opto-mechanical design

Here we show a simple example of the optimization procedure. Within the framework of a feasibility study for a robotic 3m class telescope, equipped with VIS and NIR instruments, able to react to a satellite trigger in less than 50 sec (with a goal of 30 sec): CODEVISIR (Conceptual Design for a VISible and nIR telescope), we exploited the optimization procedure to define the thickness of the main bench of the instrumental suite[15].

The instrument includes seven camera able to cover the wavelength range from the Visible (VIS, $0.4 - 0.9\mu m$) to the Near Infrared (NIR, $1 - 2.5\mu m$) during the same exposure. This will be allowed by a multichannel imaging configuration that envisages a detector for each photometric band, delivered through a dichroic cascade along the optical path. Two ancillary instruments will complete the instrumentation suite, a visible spectrograph and a photo-polarimeter, fed by rotating the M3 mirror.

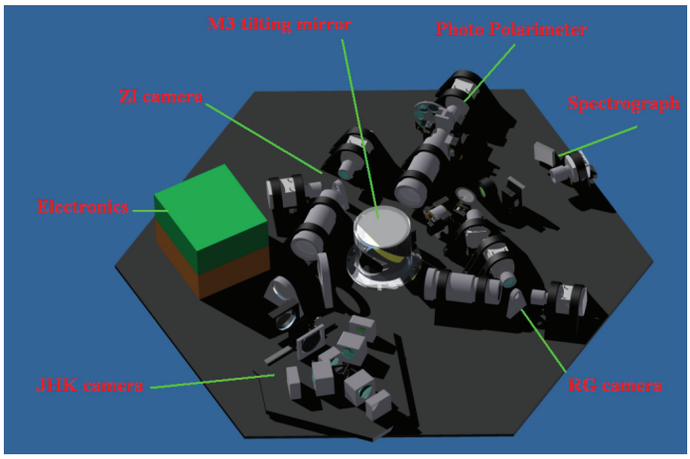

Figure 33. Codevisir Instrument suite

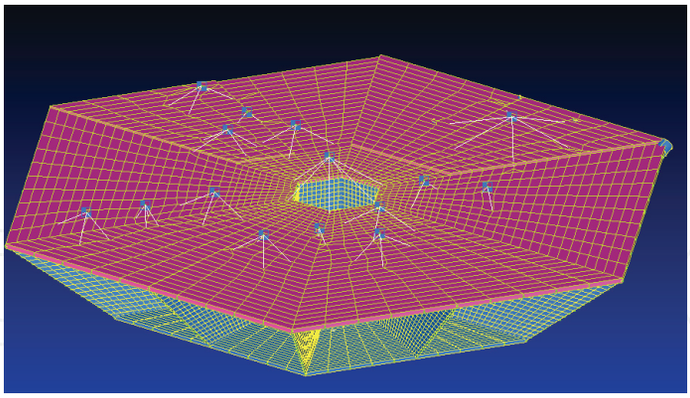

Figure 34. Finite Element simplified Model

The Optimization procedure has been oriented to weight minimizing of the overall system keeping the optical displacement[5] below proper requirements. The design variable considered is the thickness of the bench. In Figure 35 can be observed the image displacement behavior calculated as $D = \sqrt{\Delta X^2 + \Delta Y^2}$. The requirement was set at one fifth of a pixel (i.e. $3\mu m$) and the optimization variable has been modified starting from $35mm$. The optimization routine converges to a reasonable value (the thickness variation is less than a reasonable value

[5] of one of the seven arms that is also representative of the performances of all the others

($\Delta th = 0.016mm$)) within 10 steps. The final thickness is around $25mm$ and the optimized weight of the instrument is quite less than $1.2Ton$ and the final displacement is $2.88\mu m$. This procedure produce an overall weight saving of $270Kg$, starting from a very conservative value.

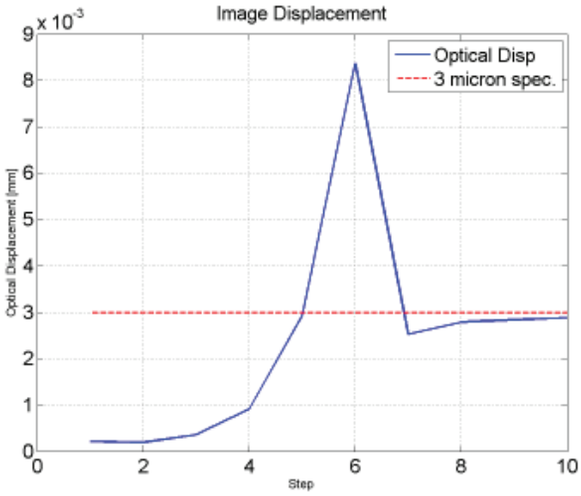

Figure 35. Image Displacement optimization

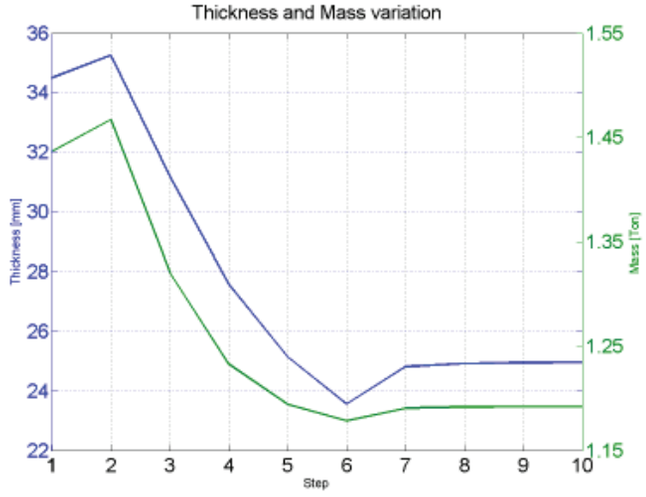

Figure 36. Thickness and Mass Variation

5. Conclusions

The aim of this chapter was to present the design procedure developed to the numerical capabilities of modern softwares and hardwares. The framework is very versatile and can be used simply for performance prediction of optical system or structres and/or for optimization strategies. The Matlab® code works as a "server" that interact with the "client" Finite Element (ABAQUS, Nastran, ...) solver managing the input file and extracting the results; the data are modified in order to be handled by the "client" raytracing software that evaluates the optical performances. The procedure is under development and integration in order to allow a multi-variable optimization. We are planning also to evaluates different optimization algorithms exploiting in particular the sensitivities analyses[5] capabilities of both Finite Element and raytracing softwares.

Author details

Marco Riva

I.N.A.F. - Osservatorio Astronomico di Brera, Italy

6. References

[1] *ABAQUS keyword reference manual* [2007].
[2] Ahmad, A. [1999]. *Handbook of Optomechanical Engineering*, CRC Press.
[3] Bettini, P., Riva, M., Sala, G., DiLandro, L., Airoldi, A. & Cucco, J. [2009]. Carbon fiber reinforced smart laminates with embedded sma actuators-part i: Embedding techniques and interface analysis, *Journal of Materials Engineering and Performance* 18(5-6): 664–671.
[4] DiSanzo, D. [2009]. *Studio di pannelli attivati da mfc: modellazione numerica e prove sperimentali*, Master's thesis, Politecnico di Milano.
[5] Doyle, K., Genberg, V. & Michels, G. [2002]. *Integrated Optomechanical Analysis*, SPIE Press.
[6] *MSC.Nastran: User guide* [2004].
[7] Riva, M. [2010]. *Smart Structures in Instrumentation for Astronomy*, PhD thesis, Aerospace Engineering, Politecnico di Milano.
[8] Riva, M. [2011]. *Smart Structures in Instrumentation for Astronomy*, LAP LAMBERT Academic Publishing.
[9] Riva, M., Bettini, P., DiLandro, L. & Sala, G. [2009]. Shape memory composite deformable mirrors, Vol. 7288, SPIE, pp. 72881T–1/72881T–12.
[10] Riva, M., Bettini, P., DiLandro, L., Sala, G. & Airoldi, A. [2009]. Carbon fiber-reinforced smart laminates with embedded sma actuators-part ii: Numerical models and empirical correlations, *Journal of Materials Engineering and Performance* 18(5-6): 672–678.
[11] Riva, M., Bettini, P., DiLandro, L., Sala, G. & Zerbi, F. [2010]. Smart structures for deformable mirrors actuated by shape memory alloy, Vol. 7739, SPIE, pp. 77391M–1/77391M–20.
[12] Riva, M., DeCaprio, V., Spanó, P. & M.Tintori [2010]. Integrated fiĄnite element analysis and raytracing, oriented to structural optimization, for astronomical instrument design, Vol. 7738, SPIE, pp. 77380J–2/77380J–9.
[13] Riva, M., DiSanzo, D., Airoldi, A., Sala, G. & Zerbi, F. [2010]. Smart structures for deformable mirrors actuated by piezocomposites, Vol. 7739, SPIE, pp. 77391N–1/77391N–16.
[14] Vanderplaats, G. [2007]. *Multidiscipline design optimization*, VR&D Press.
[15] Vitali, F., Chincarini, G., M.Zannoni & all. [2010]. A path to the stars: the evolution of the species in the hunting to the grbs, Vol. 7730, SPIE, pp. 77330W–1/ 77330W–14.
[16] Wilkie, W., Bryant, G. & et all, J. H. [2000]. Low cost piezocomposite actuator for structural control applications, *7th Annual International Symposium on Smart Structures and Materials*, SPIE, Newport Beach.
[17] *ZEMAX: Optical Design Program User's Guide* [2005].